Termination of Biological Function at Low Temperatures: Glass or Structural Transition?

Journal:	*The Journal of Physical Chemistry Letters*
Manuscript ID	jz-2018-00537c.R1
Manuscript Type:	Letter
Date Submitted by the Author:	n/a
Complete List of Authors:	Seyedi, Salman; Arizona State University, Physics Matyushov, Dmitry; Arizona State University, Chemistry and Biochemistry

Termination of Biological Function at Low Temperatures: Glass or Structural Transition?

Salman Seyedi† and Dmitry V. Matyushov*,‡

†*Department of Physics, Arizona State University, PO Box 871504, Tempe, Arizona 85287*

‡*Department of Physics and School of Molecular Sciences, Arizona State University, PO Box 871504, Tempe, AZ 85287-1504*

E-mail: dmitrym@asu.edu

Abstract

Energy of life is produced by electron transfer in energy chains of respiration or photosynthesis. A small input of free energy available to biology puts significant restrictions on how much free energy can be lost in each electron-transfer reaction. We advocate the view that breaking ergodicity, leading to violation of the fluctuation-dissipation theorem (FDT), is how proteins achieve high reaction rates without sacrificing the reaction free energy. Here we show that a significant level of nonergodicity, represented by a large extent of the configurational temperature over the kinetic temperature, is maintained in the entire physiological range for the cytochrome *c* electron transfer protein. The protein returns to the state consistent with the FDT below the crossover temperature close to the temperature of the protein glass transition. This crossover leads to a sharp increase in the activation barrier of electron transfer and is displayed by a kink in the Arrhenius plot for the reaction rate constant.

Graphical TOC Entry

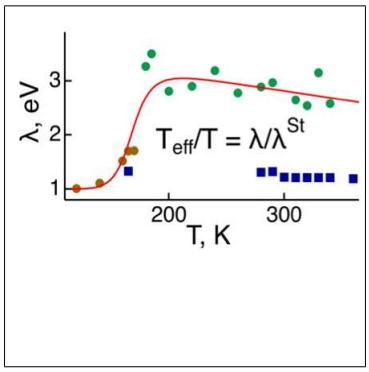

Life exists in a very narrow range of temperatures and the question of what happens when the temperature is lowered seems to be irrelevant for biological function. However, in particular in the field of physiological energy flow,[1] lowering temperature has offered significant insights into the basic physical mechanisms behind the high-temperature phenomena. The classical experiments by de Vault and Chance[2] showed that the rate of protein electron transfer becomes temperature-independent below ~ 150 K, which helped to realize that electron tunneling is the physical mechanism behind biological electron transport.[3] Likewise, lowering temperature in Mössbauer spectroscopy of myoglobin allowed Parak and Formaneck[4] to observe a kink in the temperature dependence of iron displacement in the heme cofactor. This result came in violation of the fluctuation-dissipation theorem (FDT)[5] and of an even earlier result known as the Nyquist theorem.[6] Here, we continue along this path of enquiry by employing large-scale molecular dynamics (MD) simulations to drive cytochrome *c* (Cyt-c) protein below its glass transition to interrogate the effect of lowering temperature on the activation barrier of protein electron transfer. We show that the violation of the FDT first pointed out by Parak and Formaneck[4,7] is a fundamental principle allowing proteins to achieve fast reaction rates without sacrificing the reaction free energy.

The FDT is a set of relations connecting the response of a macroscopic variable X to a weak perturbation with thermal fluctuations of the same variable.[5] Specifically, if a weak step perturbation F is introduced at time $t = 0$, the change $\Delta X(t) = \chi(t)F$ is represented by the product of the linear response function $\chi(t)$ and F. The total change $\Delta X(\infty)$ obtained at $t \to \infty$ is related to the variance $\langle \delta X^2 \rangle$ caused by thermal agitation at equilibrium:[5] $k_{\mathrm{B}} T \chi(\infty) = \langle \delta X^2 \rangle$ (angular brackets refer to an equilibrium ensemble average).

The general framework of the FDT applies to solvation of charge by polar liquids and is typically ascribed to the linear response approximation for solvation,[8] with the most famous result given by the Born equation for polar solvation. This framework is also commonly applied to enzymology[9,10] and, more specifically, to probably the simplest reaction catalyzed by proteins, the reaction of electron transfer.[1,11] No bonds are formed or broken during electron transfer, which allows one to reduce the problem to the language of nonequlibrium solvation and the fluctuation-dissipation re-

lations. This connection was achieved by Marcus,[12] who, following Onsager's idea of microscopic reversibility,[13] defined the free energy required to bring the donor and acceptor in the resonance configuration for electron tunneling. This formalism has lead to now widely accepted picture of equal-curvature crossing parabolas (Figure 1). The collective variable $X = \Delta E(\mathbf{q})$, depending on the system's nuclear coordinates $\mathbf{q}$, is the energy gap between the initial and final electronic states[14] and the activation barrier is the free energy required to climb from the parabola's bottom to $X = 0$ at the crossing point (tunneling configuration).

While providing a general and widely applicable view of activated processes in polar materials, the Marcus picture is too limited when applied to protein electron transfer. The difficulty is the need for a large in magnitude and negative reaction free energy,[11] $\Delta G_0 \simeq -\lambda$, to accomplish sufficiently fast near-activationless electron transfer often observed in primary events of photosynthesis and energy chains of respiration.[15,16] The proposal that proteins might provide a weakly polar environment for redox active sites[17] has been mostly refuted by a large number of recent MD simulations[18] and by comparison of simulations with experiment[19–21] (with potential exceptions of active sites buried deep inside the membrane-bound proteins[18,22]). As our simulations below also indicate, the typical reorganization energy of protein electron transfer, $\simeq 1$ eV, is not much different from the standard expectations for organic donor-acceptor complexes in solution[23,24] and ligand-protected (e.g., $\lambda \simeq 1$ eV for cobaltocene[25]) redox metal ions (up to three times higher reorganization energies are found for transition metal aqua ions[26]). Such relatively high values of the reorganization energy for protein electron transfer require significant losses of free energy for an energy chain operating at low activation barriers. On the other hand, rather small input free energy, $|\Delta G_0| \simeq 1$ eV, is typically available to biology, either through the photon energy or the redox potential of organic molecules.[1] Since this input needs to be utilized in a large number of electron-transfer steps, energy complexes of biology must have developed non-Marcusian mechanisms of operation to avoid wasteful conversion of free energy to heat.

Nonlinear solvation, going beyond the linear response approximation of the Marcus picture and the FDT, does not seem to have a significant chance to operate in the soft environment of an active

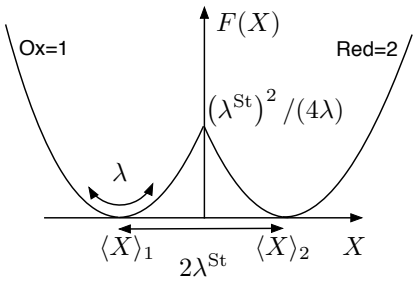

Figure 1: Schematic representation of the free energy surfaces for half electron transfer, $\mathrm{Ox} + \mathrm{e}^- \rightarrow \mathrm{Red}$. The oxidized ($\mathrm{Ox} = 1$) and reduced ($\mathrm{Red} = 2$) states are characterized by approximately parabolic free energy surfaces along the energy gap reaction coordinate X, with the minima at $\langle X\rangle_1$ and $\langle X\rangle_2$. The separation between the minima is twice the Stokes-shift reorganization energy λ^{St}. The curvatures of the parabolas produce the reorganization energy λ related to the variance of X: $\lambda = \langle \delta X^2\rangle/(2k_{\mathrm{B}}T)$. The activation barrier of a half reaction is determined by crossing of two parabolas at $X = 0$ and is given by eq 2 at zero reaction free energy.

site subjected to screening by mobile waters and ionic clouds.[8,27] We have alternatively suggested that energetic efficiency of biology exceeding the predictions of the standard models is achieved by eliminating ergodicity,[19] i.e., by incomplete sampling of the space of available configurations. This hypothesis leads to a number of verifiable predictions.[28] Most directly, ergodicity breaking, common to glass science, leads to the violation of the FDT with the consequence that the thermal variance of an observable property $\langle \delta X^2\rangle/(k_{\mathrm{B}}T)$ exceeds the linear susceptibility $\chi(\infty)$. To characterize this distinction, one introduces an effective (fictive[29]) temperature of a glassy system $T_{\mathrm{eff}} \propto \langle \delta X^2\rangle/\chi(\infty)$.[30–33] In the case of electron transfer, this definition translates to the following relation[28]

$$\frac{T_{\mathrm{eff}}}{T} = \frac{\lambda}{\lambda^{\mathrm{St}}} \tag{1}$$

Here, T_{eff} is the effective temperature characterizing the configurational manifold of the thermal bath of the reaction site (protein an the surrounding solvent for protein electron transfer) and T is the standard kinetic temperature.

The right-hand side of eq 1 involves two reorganization energies, λ^{St} and λ. The former is the analog of the linear susceptibility $\chi(\infty)$ of the FDT. It is equal to half of the separation between the mean values of the energy gap X in two electron-transfer states[34,35] (the Stokes shift[36]): $\lambda^{\mathrm{St}} = |\langle X\rangle_2 - \langle X\rangle_1|/2$ (Figure 1). The second reorganization energy is determined by the variance of

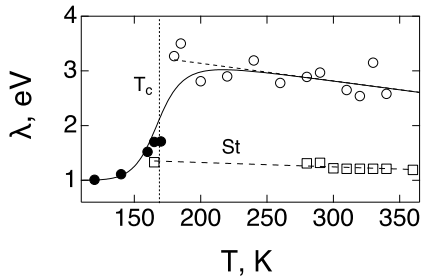

Figure 2: Temperature dependence of the reorganization energies calculated from the first and second moments of the reaction coordinate, λ^{St} (marked as "St", open squares) and λ (circles). We find $\lambda \gg \lambda^{\mathrm{St}}$ at high temperatures (open circles), in violation of the fluctuation-dissipation theorem, and the return to $\lambda^{\mathrm{St}} \simeq \lambda$ anticipated by the FDT below the crossover temperature $T_c \simeq 170$ K (filled circles). The results for λ refer to the oxidized state of Cyt-c, and both oxidized and reduced states were simulated to produce λ^{St}. The solid curve is the fit to eq 9 assuming ergodicity breaking with the Arrhenius relaxation time $\tau_X = \tau_0 \exp[E_X/(k_{\mathrm{B}}T)]$. The activation energy $E_X/k_{\mathrm{B}} = 1725$ K was obtained from MD simulations (Figure S3 in the SI) and $\tau_0/\tau_{\mathrm{obs}} = 10^{-6}$ was adopted based on the length of the simulation trajectories. The dashed lines are the linear regressions through the simulation points.

X, $\lambda = \langle \delta X^2 \rangle / (2k_{\mathrm{B}}T)$, and provides the curvature for two crossing parabolas, $F(X) = (X \pm \lambda^{\mathrm{St}})^2/(4\lambda)$, shown in Figure 1.

In the thermodynamic limit of ergodic sampling described by the FDT, $T_{\mathrm{eff}} = T$ and $\lambda^{\mathrm{St}} = \lambda$, as required by the standard theory.[11] When ergodicity is broken, one gets[31] $T_{\mathrm{eff}} > T$ and the reorganization energy from the curvature exceeds that from the shift between the parabolas' minima. As is easy to appreciate from Figure 1, this scenario leads to the drop of the activation barrier compared to the standard theory. The activation barrier with zero reaction free energy becomes

$$\Delta F^{\dagger} = \lambda^r/4 = \left(\lambda^{\mathrm{St}}\right)^2/(4\lambda) = (\lambda^{\mathrm{St}}/4)\,(T/T_{\mathrm{eff}}) \tag{2}$$

The effective "reaction" reorganization energy λ^r is the only parameter that enters the activation barrier, which for a non-zero reaction free energy ΔG_0 still carries the form of the Marcus theory[28]

$$\Delta F^{\dagger} = (\Delta G_0 + \lambda^r)^2/(4\lambda^r) \tag{3}$$

What is different from the standard theory is that $\lambda^r = (\lambda^{\mathrm{St}})^2/\lambda$ loses its simple meaning of a linear

solvation free energy and becomes a composite parameter given by eq 2. In the case of Cyt-c at 300 K we obtain from MD simulations: $\lambda \simeq 2.9$ eV, $\lambda^{\rm St} \simeq 1.3$ and $T_{\rm eff}/T \simeq 2.3$. The resulting $\lambda^r \simeq 0.57$ eV is in close agreement[21] with the values reported from electrochemistry of proteins attached to monolayer-coated electrodes,[37–39] $\lambda^r \simeq 0.58 \pm 0.04$ eV. This result is slightly below $\lambda^r \simeq 0.7$ eV from solution rates measured vs the reaction driving force (Marcus inverted parabola) for cytochrome *c* proteins modified through the attachment of electron donors.[26]

Mechanisms to lower the reaction barriers had to be sought after by natural selection. Our theoretical framework presents a potential realization of this selection pressure through a physically robust mechanism. The practical question is whether proteins can serve as media allowing ergodicity breaking and what are the magnitudes of barrier depression that can be achieved.

The main result of this study is shown in Figure 2. It presents the analysis of extensive ($> 5.6\,\mu$s) MD simulations of Cyt-c (PBD 1GIW and 1AKK) in two redox states at a number of temperature from above the room temperature ($T_{\rm H} = 360$ K) to low temperatures ($T_{\rm L} = 120$ K) below the glass transition of the protein at $T_g \simeq (170 - 180)$ K.[40] The main observation from these data is that

$$T_{\rm eff} \gg T \tag{4}$$

at physiological temperatures, where $\lambda(T)$ is a slightly dropping function of temperature, as expected.[41] The high-temperature behavior, where the FDT is clearly violated, is followed by a sharp return to the FDT expectations, $T_{\rm eff} \simeq T$, at a crossover temperature T_c not too far from T_g. The question addressed by this report is what are the mechanisms contributing to this unusual phenomenology. The simulation protocol for the MD simulations presented here was described previously[21,42] and is discussed in more detail in the Supporting Information (SI). It is important to note that while $T_{\rm eff} \gg T$ is often found for the electrostatics of protein active sites in agreement with experimentally reported kinetics of electron transfer,[19,20] Cyt-c is a somewhat special case. We found, in agreement with previous simulations,[18,43] that $\lambda \simeq \lambda^{\rm St}$ when the heme is represented by partial atomic charges and no polarizability of the active site is included. The condition

$\lambda \gg \lambda^{\mathrm{St}}$ is achieved by allowing polarizability of the active site modeled here by QM/MD calculations described in previous publications[21,42] and in the SI. The polarizability of Cyt-c significantly exceeds what a similar formalism finds for iron-sulfur clusters in bacterial complex I, where still $T_{\mathrm{eff}}/T \approx 3-6$ was reported.[44]

One first has to stress that the ratio $T_{\mathrm{eff}}/T > 2$ is significantly higher for proteins than for bulk glass-formers,[32] but close to the results obtained by pulling DNA hairpins with optical tweezers.[33] The DNA experiments represent a driven system, while protein electrostatics is intrinsically non-equilibrium. There are, therefore, some unique properties of the biomolecule-water thermal bath that allow a very substantial deviation from the FDT for the charge-potential conjugate variables and a correspondingly large depression of the activation barrier related to electrostatics at the active site. As mentioned above, the ratios $T_{\mathrm{eff}}/T > 2$ found for a number of proteins are consistent with experimental observations for bacterial photosynthesis[19,28] and electrochemistry of the Cyt-c.[21]

The first question to ask in connection with a sharp drop of λ at T_c is whether one can identify some other properties, related either to the protein or to its hydration shell, which show similarly strong alterations around T_c. We could not identify protein properties showing a crossover, but a number of crossovers for the hydration shell were found by the present simulations.

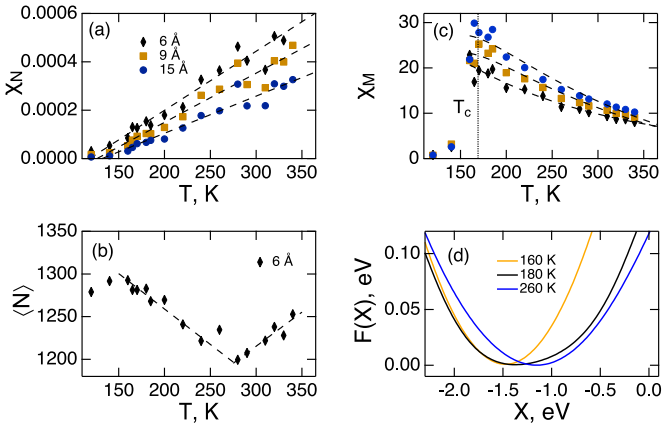

Figure 3: (a) Compressibility of hydration shells $\chi_N(a)$ (eq 5). (b) Average number of water molecules in the shell of thickness $a = 6$ Å. (c) Dipolar susceptibility $\chi_M(a)$ (eq 6). (d) Free energy surfaces of oxidized Cyt-c (eq 7), $F(X) = F_1(X)$. The free energy surfaces have been shifted to the common level $F(\langle X\rangle_1) = 0$. The dashed lines drawn through the points in (a)-(c) are fits to guide the eye and the vertical dotted line in (c) is drawn at the temperature $T_c \simeq 170$ K also shown in Figure 2.

We first focus on whether the orientational or density manifold of the hydration shell shows an unusual behavior. Figure 3a presents the compressibility of the hydration layers of different thickness a measured from the protein's van der Waals surface. The compressibility is calculated as the variance relative to the average number of hydration waters in the shell of thickness a[45–47]

$$\chi_N(a) = \langle \delta N(a)^2 \rangle / \langle N(a) \rangle \tag{5}$$

The resulting functions $\chi_N(a)$, calculated for $a = 6, 9, 15$ Å, are all approximately proportional to the kinetic temperature T, as expected from the FDT (Figure 3a). No discontinuity is seen at T_c, even though a curious dependence is found for the average number of waters, as is shown in Figure 3b. The average $\langle N(a) \rangle$ is seen to go through a minimum at $T \simeq 270$ K. It is also reflected by a slight bump of $\chi_N(T)$ at the same temperature. The origin of this behavior is not clear since TIP3P force field used in the simulations does not display the density maximum consistent with the properties of water. The compressibility of the hydration shell is also higher for thinner shells, despite a typically higher density of the hydration water compared to the bulk.[48] This observation indicates that the network of water hydrogen bonds is broken in the hydration shell (see also below), which is therefore more disordered than the bulk[49,50] and has a higher compressibility.

The temperature dependence of the orientational manifold of the hydration water is distinctly different from its density. Figure 3c shows the dipole moment susceptibility[47]

$$\chi_M(a) = [3 v_w k_{\mathrm{B}} T \langle N(a) \rangle]^{-1} \langle \delta \mathbf{M}(a)^2 \rangle \tag{6}$$

Here, $v_w = (\pi/6)\sigma_w^3$, $\sigma_w = 2.87$ Å is the volume of a single water molecule and $\mathbf{M}(a)$ is the dipole moment of the water molecules in the shell of thickness a and $\delta\mathbf{M}(a) = \mathbf{M}(a) - \langle \mathbf{M}(a) \rangle$. The dimensionless dipolar susceptibility is defined in analogy with the dielectric susceptibility of bulk dielectrics.[51] It is normalized with the average number of waters in the shell $\langle N(a) \rangle$. The temperature dependence of $\chi_M(a)$ is peculiar in two regards: (i) it violates the FDT even at high temperatures (similarly to $\lambda(T)$ in Figure 2), increasing with lowering temperature in contrast to

the anticipated decrease, and (ii) it shows a sharp drop to nearly zero at a temperature consistent with the drop of λ at T_c (vertical dotted line in Figure 3c). The violation of the temperature dependence predicted by the FDT for the variance of the bulk dipole moment is displayed by many polar liquids,[52] but the temperature slope of $\chi_M(a)$ for the hydration shells far exceeds that for bulk liquids. A similar observation was previously made for the lysozyme protein,[47] and this behavior of $\chi_M(T)$ might universally apply to the protein hydration shells.

The question raised by the unusual temperature dependence of $\chi_M(T)$ is whether the hydration shell is en route to a dipolar ordered phase interrupted by the glass transition, similarly to the phenomenology found for relaxor ferroelectrics.[53] We have analyzed orientational order of the interfacial dipoles in terms of two lowest order parameters, $p_l = \langle P_l(\cos\theta)\rangle$, $l = 1, 2$, of the water dipoles forming the angle θ with the closest normal direction to the van der Waals surface of the protein[47] ($P_l(x)$ is the Legendre polynomial of order l). The preferential alignment of water molecules in the interface corresponds to their hydrogens pointing toward the protein surface (either dangling OH bonds[54,55] or hydrogen bonds with the protein, Figure S6 in the SI). This alignment, which is further tested with a separate order parameter[56] p_{21} sensitive to dangling bonds (Figure S7 in the SI), is enhanced when the temperature is lowered (Figure S5 in the SI). Nevertheless, there is no distinguishable structural transition in the ordering of dipoles in the interface. Still, the free energy surfaces of electron transfer presented in Figure 3d indicate a bimodal behavior near T_c.

The free energy surfaces of electron transfer define the free energy required to bring the system to a specific value of the energy gap X between the initial and final electron energies. For the half reaction changing the oxidation state of Cyt-c, the energy gap $\Delta E(\mathbf{q})$ is between the electronic states of the oxidized and reduced states of the heme cofactor.[21] The free energy surface is defined by tracing out the entire manifold of the nuclear degrees of freedom $\mathbf{q}$ while restraining the energy gap to a given value X

$$e^{-F(X)/(k_{\mathrm{B}}T)} \propto \langle \delta\left(X - \Delta E(\mathbf{q})\right)\rangle \tag{7}$$

The details of the calculation formalism are given in the SI. Briefly, we employ Warshel's valence-bond approach,[57,58] in which the quantum-mechanical Hamiltonian of the heme with lig-

ating amino acids is diagonalized at each simulation frame along the MD trajectory.[42,43] The energies produced by diagonalizing the oxidized and reduced states of Cyt-c form the energy gap $X = \Delta E(\mathbf{q})$. The distributions $P_i(X)$ directly lead to the free energy surfaces $F_i(X) = -k_{\mathrm{B}}T \ln[P_i(X)]$ ($1 =$ Ox and $2 =$ Red, Figure 1). Correspondingly, the first moments of the distribution $\langle X \rangle_{1,2}$ are used to calculate λ^{St} and the second cumulant $\langle \delta X^2 \rangle_1$ leads to the reorganization energy λ in the oxidized state shown in Figure 2. Finally, the free energy surfaces for the oxidized state of Cyt-c at different temperatures are shown in Figure 3d. They show a distinct shift of the minimum around T_c, with the overall shape near T_c suggestive of a bimodal distribution (similarly to Landau's free energy functionals of an order parameter[59]). In search of a possible structural transition[60] of water in the protein-water interface, we have examined the temperature effect on the distribution functions $P(Q)$ of the tetrahedral order parameter Q of hydration water.

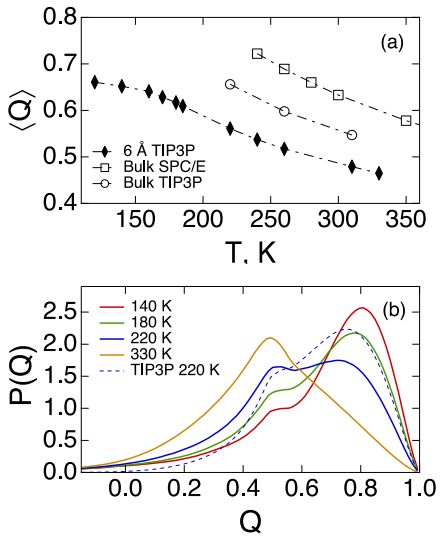

Figure 4: (a) $\langle Q \rangle$ vs T for the hydration waters within the shell of thickness $a = 6$ Å around Cyt-c in the oxidized form (filled diamonds). Also shown are $\langle Q \rangle$-values for bulk SPC/E water[61] (open squares) and TIP3P water (open circles). (b) Distribution functions of the tetrahedral order parameter[62,63] (eq 8) in the hydration shell of oxidized Cyt-c ($a = 6$ Å) at different temperatures. The dashed line refers to bulk TIP3P water.

The tetrahedral order parameter[62,63]

$$Q = 1 - \tfrac{3}{8} \sum_{i=1}^{3} \sum_{j=i+1}^{4} \left(\cos\theta_{ij} + 1/3\right)^2 \tag{8}$$

is defined by the angle θ_{ij} formed by a target molecule with its four nearest neighbors i and j. Tetrahedral ice-like structure yields $\langle Q \rangle = 1$ and $\langle Q \rangle = 0$ describes the state of orientational disorder. We find that $\langle Q \rangle$ of the hydration shell increases monotonically with lowering temperature (Figure 4a) in parallel to bulk SPC/E[61] and TIP3P water, but below both of them. Consistently with compressibility $\chi_N(a)$ of hydration shells (Figure 3a), lower $\langle Q \rangle$ values indicate higher disorder of hydration water compared to the bulk.[49,50] The distributions $P(Q)$ shown in Figure 4b rather closely follow the behavior observed in the bulk[63] (dashed line), developing a bimodal distribution pointing to a more ordered hydration water at low temperatures (also see Figure S4 in the SI). The disturbance of the tetrahedral order imposed by the protein is marginal[64] and, overall, we see little evidence of a structural transition of the hydration shell around the crossover temperature. We therefore favor the glass transition (dynamical freezing) interpretation of the crossover in both λ and χ_M. The two-state shape of $F(X)$ near the crossover temperature (Figure 3d) likely reflects changes in the bimodal distribution of Q shown in Figure 4b.

In the glass transition scenario, thermal motions of the medium, leading to fluctuations of the electron-transfer energy gap X, become dynamically frozen when the relaxation time $\tau_X(T)$ of the collective coordinate $X(t)$ becomes comparable with the observation time τ_{obs}, which is the length of the simulation trajectory in our case. In turn, the relaxation time $\tau_X(T)$ is associated with the Stokes-shift dynamics[36] and is found from the corresponding Stokes-shift time correlation function $C_X(t) = \langle \delta X(t) \delta X(0) \rangle$, $\delta X(t) = X(t) - \langle X \rangle$. The nonergodic reorganization energy becomes a sum of the low-temperature component λ_f produced by fast vibrational and ballistic motions of the medium and the component λ_s related to collective medium fluctuations with the relaxation time $\tau_X(T)$. The slow component λ_s is multiplied by the nonergodicity factor accounting for dynamical

freezing[28]

$$\lambda(T) = \lambda_f + (2\lambda_s/\pi)\cot^{-1}\left[\tau_X(T)/\tau_{\rm obs}\right] \quad (9)$$

The results of MD simulations for $\tau_X(T)$ were fitted to the Arrhenius law $\tau_X = \tau_0 \exp[E_X/(k_{\rm B}T)]$ yielding $E_X/k_{\rm B} \simeq 1725$ K (Figure S3 in the SI). This relaxation time was then used in eq 9 to produce the solid line in Figure 2 based on the low-temperature value λ_f and the high-temperature linear interpolation of the simulation points (upper dashed line in Figure 2). The crossover temperature $T_c \simeq 170$ K (vertical dotted line in Figure 2) is determined as the mean point $\lambda(T_c) = (\lambda_s + \lambda_f)/2$. We reach an overall consistency of this procedure, and the hypothesis of dynamical freezing, with the simulation data.

The data accumulated in this study present the following general picture of kinetically and energetically efficient operation of redox enzymes. The folded state of the protein, strongly coupled with the surrounding hydration water, exists in a nonergodic state similar to a quenched and ageing glass.[65] The resulting incomplete sampling of the phase space leads to a separation of the configurational effective temperature $T_{\rm eff}$ from the kinetic temperature T, eq 1. In contrast to bulk glass formers, where the excess of $T_{\rm eff}$ over T is very minor, this ratio can be very significant, $T_{\rm eff}/T \simeq 2-6$, when judged from $\lambda^{\rm St}$ and λ.[19,28] The excess amplitude of fluctuations, leading to large magnitudes of λ, is provided by coupled fluctuations of the protein-water interface.[19] The time-scale of these fluctuations is on the scale from hundreds of picoseconds to nanoseconds to microseconds.[66] The Stokes-shift relaxation time follows the Arrhenius temperature dependence with the activation barrier $E_X/k_{\rm B} \simeq 2 \times 10^3$ K consistent with β-type relaxation of the protein hydration shell.[67]

Coupled protein-water fluctuations can be dynamically frozen by either choosing a reaction window τ_r significantly below τ_X, or by lowering temperature and thus driving $\tau_X(T)$ out of the observation window. The former mechanism is accomplished for fast primary reactions of bacterial photosynthesis,[16,19] where the reaction time is $\tau_r \simeq 3-10$ ps. The latter mechanism is explored by us in this paper for protein electron transfer. We have previously shown that the same mechanism applies to the dynamical transition in proteins,[4] when lowering temperature drives the dynamics

of heme's iron displacements out of the observation window.[68] When the collective modes of the protein-water interface, allowing nonergodic sampling of configurations, freeze in, only fast ballistic modes of the thermal bath drive thermal fluctuations. The reaction kinetics returns at this point to the expectations of the FDT. In the framework of electron-transfer kinetics, this regime corresponds to equality of two reorganization energies, $\lambda^{\mathrm{St}} \simeq \lambda$, as we indeed observe in MD simulations (Figure 2).

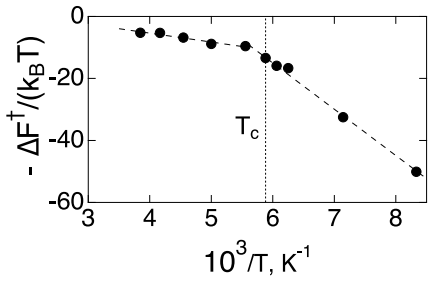

Figure 5: Arrhenius plot of $-\Delta F^{\dagger}/(k_{\mathrm{B}}T)$ vs $1/T$ for the reaction of electrode reduction of Cyt-c. Points represent the activation barriers calculated as $\Delta F^{\dagger} = F(0) - F(\langle X \rangle_1)$ from the free energy surfaces calculated at different temperatures from MD trajectories. The dashed lines are linear interpolations between the points. The vertical dotted line indicates the crossover temperature T_c shown in Figure 2.

An observable consequence of the sharp return of the protein to the ergodic behavior at lower temperatures should be displayed as a crossover in the Arrhenius plot for the reaction rate. This is illustrated in Figure 5 where we calculated the activation barrier of electron transfer as the free energy required to reach the activated state $X = 0$, $\Delta F^{\dagger} = F(0) - F(\langle X \rangle_1)$. The free energy surfaces at different temperature were obtained from MD simulations according to eq 7. The sharp drop of λ at T_c is accompanied by an increase in the slope of the Arrhenius plot (the activation energy vs $1/T$ is shown in Figure S8 in the SI).

Crossovers in Arrhenius plots are far from unusual for photosynthetic systems.[69–71] The earliest examples are the classical experiments by de Vault and Chance,[2] where flattening of the Arrhenius plot for electron transfer from reduced Cyt-c to the primary reaction center donor at low temperatures was reported. It is therefore important to stress that many of these reactions involve the reaction free energy, with its own temperature dependence,[19] and are often close to activationless[15]

or electron-transfer inverted regimes, when intramolecular vibrations become significant, particularly at low temperatures.[17] In contrast, Figure 5 shows activated kinetics in the normal regime of electron transfer, not affected by quantum intramolecular vibrations and for a half (electrode) reaction with no driving force (zero overpotential for electrochemistry). The activation barrier, and its increase at lower temperatures, are solely the result of two reorganization energies in eq 2.

The perspective presented here offers a potential explanation for the evolutionary pressure preserving large protein complexes to drive electron transport in biological energy chains. Obviously, redox chemistry can be accomplished by much smaller molecules, such as organic donor-acceptor complexes employed in photoinduced electron transfer.[23] However, the Stokes-shift dynamics of small molecules, leading to electron transfer, are extremely fast in water,[72] with most of the Stokes shift accumulated at sub-picosecond times. This is the case of $\tau_X \ll \tau_r$, when ergodic conditions are fulfilled and no rate increase due to reaction nonergodicity can be achieved. In contrast, for large protein complexes, a significant portion of the Stokes shift is associated with much longer time-scales, in the nanosecond to microsecond domain.[66] These large complexes, due to a combination of properties not fully understood and distinct from bulk glass formers,[32] allow highly nonergodic sampling of the reaction coordinate, thus leading to the configurational temperature much exceeding the kinetic temperature (eqs 1 and 4).

Acknowledgement

This research was supported by the National Science Foundation (CHE-1800243). CPU time was provided by the National Science Foundation through XSEDE resources (TG-MCB080071).

Supporting Information Available

Simulation protocols and calculation procedures for the reorganization energies of electron transfer and order parameters of the hydration shell discussed in the text. This material is available free of charge via the Internet at `http://pubs.acs.org/`.

References

(1) Nicholls, D. G.; Ferguson, S. J. *Bioenergetics 3*; Academic Press: London, 2002.

(2) de Vault, D.; Chance, B. Studies of phosynthesis using a pulsed laser. I. Temperature dependence of cytochrome oxidation rate in Chromatium. Evidence for tunneling. *Biophys. J.* **1966**, *6*, 825.

(3) Skourtis, S. S.; Waldeck, D. H.; Beratan, D. N. Fluctuations in biological and bioinspired electron-transfer reactions. *Annu. Rev. Phys. Chem.* **2010**, *61*, 461–485.

(4) Parak, F.; Formanek, H. Untersuchung des Schwingungsanteils und des Kristallgitterfehleranteils des Temperaturfaktors in Myoglobin durch Vergleich von Miissbauerabsorptionsmessungen mit Riintgenstrukturdaten. *Acta Crystallogr. A* **1971**, *27*, 573.

(5) Kubo, R. The fluctuation-dissipation theorem. *Rep. Prog. Phys.* **1966**, *29*, 255–284.

(6) Nyquist, H. Thermal agitation of electric charge in conductors. *Phys. Rev.* **1928**, *32*, 110–113.

(7) Parak, F. G. Physical aspects of protein dynamics. *Rep. Prog. Phys.* **2003**, *66*, 103–129.

(8) Hummer, G.; Pratt, L. R.; Garcia, A. E. Free Energy of Ionic Hydration. *J. Phys. Chem.* **1996**, *100*, 1206–1215.

(9) Warshel, A.; Parson, W. W. Dynamics of biochemical and biophysical reactions: insight from computer simulations. *Quart. Rev. Biophys.* **2001**, *34*, 563.

(10) Volkán-Kacsó, S.; Marcus, R. A. Theory of single-molecule controlled rotation experiments, predictions, tests, and comparison with stalling experiments in F 1-ATPase. *Proc. Natl. Acad. Sci. U.S.A.* **2016**, *113*, 12029–12034.

(11) Marcus, R. A.; Sutin, N. Electron transfer in chemistry and biology. *Biochim. Biophys. Acta* **1985**, *811*, 265–322.

(12) Marcus, R. A. Electrostatic free energy and other properties of states having nonequilibrium polarization. I. *J. Chem. Phys.* **1956**, *24*, 979–989.

(13) Onsager, L.; Machlup, S. Fluctuations and irreversible processes. *Phys. Rev.* **1953**, *91*, 1505–1512.

(14) Warshel, A. Dynamics of reactions in polar solvents. Semiclassical trajectory studies of electron-transfer and proton-transfer reactions. *J. Phys. Chem.* **1982**, *86*, 2218–2224.

(15) Fleming, G. R.; Martin, J. L.; Breton, J. Rates of primary electron transfer in photosynthetic reaction centers and their mechanistic implications. *Nature* **1988**, *333*, 190–192.

(16) Hoff, A. J.; Deisenhofer, J. Photophysics of photosynthesis. *Phys. Rep.* **1997**, *287*, 1–247.

(17) Bixon, M.; Jortner, J. Electron transfer – from isolated molecules to biomolecules. *Adv. Chem. Phys.* **1999**, *106*, 35.

(18) Blumberger, J. Recent advances in the theory and molecular simulation of biological electron transfer reactions. *Chem. Rev.* **2015**, *115*, 11191–11238.

(19) LeBard, D. N.; Matyushov, D. V. Protein-water electrostatics and principles of bioenergetics. *Phys. Chem. Chem. Phys.* **2010**, *12*, 15335–15348.

(20) LeBard, D. N.; Martin, D. R.; Lin, S.; Woodbury, N. W.; Matyushov, D. V. Protein dynamics to optimize and control bacterial photosynthesis. *Chem. Sci.* **2013**, *4*, 4127–4136.

(21) Seyedi, S.; Waskasi, M. M. M.; Matyushov, D. V. Theory and electrochemistry of cytochrome *c*. *J. Phys. Chem. B* **2017**, *121*, 4958–4967.

(22) Tipmanee, V.; Blumberger, J. Kinetics of the terminal electron transfer step in cytochrome *c* oxidase. *J. Phy. Chem. B* **2012**, *116*, 1876–1883.

(23) Closs, G. L.; Miller, J. R. Intramolecular long-distance electron transfer in organic molecules. *Science* **1988**, *240*, 440–447.

(24) Barbara, P. F.; Meyer, T. J.; Ratner, M. A. Contemporary issues in electron transfer research. *J. Phys. Chem.* **1996**, *100*, 13148–13168.

(25) Fawcett, W. R.; Opallo, M. Possible experimental evidence for molecular solvation effects in simple heterogeneous electron-transfer reactions. *J. Phys. Chem.* **1992**, *96*, 2920–2924.

(26) Winkler, J. R.; Gray, H. B. Electron flow through metalloproteins. *Chem. Rev.* **2014**, *114*, 3369–3380.

(27) Kuharski, R. A.; Bader, J. S.; Chandler, D.; Sprik, M.; Klein, M. L.; Impey, R. W. Molecular model for aqueous ferrous-ferric electron transfer. *J. Chem. Phys.* **1988**, *89*, 3248–3257.

(28) Matyushov, D. V. Protein electron transfer: is biology (thermo)dynamic? *J. Phys.: Condens. Matter* **2015**, *27*, 473001.

(29) Angell, C. A.; Ngai, K. L.; McKenna, G. B.; McMillan, P. F.; Martin, S. W. Relaxation in glassforming liquids and amorphous solids. *J. Appl. Phys.* **2000**, *88*, 3113–3157.

(30) Cugliandolo, L. F.; Kurchan, J.; Peliti, L. Energy flow, partial equilibration, and effective temperatures in systems with slow dynamics. *Phys. Rev. E* **1997**, *55*, 3898–3914.

(31) Nieuwenhuizen, T. M. Thermodynamics of the glassy state: Effective temperature as an additional system parameter. *Phys. Rev. Lett.* **1998**, *80*, 5580–5583.

(32) Grigera, T. S.; Israeloff, N. E. Observation of fluctuation-dissipation-theorem violations in a structural glass. *Phys. Rev. Lett.* **1999**, *83*, 5038–5041.

(33) Dieterich, E.; Camunas-Soler, J.; Ribezzi-Crivellari, M.; Seifert, U.; Ritort, F. Single-molecule measurement of the effective temperature in non-equilibrium steady states. *Nature Phys.* **2015**, *11*, 971–977.

(34) Muegge, I.; Qi, P. X.; Wand, A. J.; Chu, Z. T.; Warshel, A. The reorganization energy of cytochrome c revisited. *J. Phys. Chem. B* **1997**, *101*, 825–836.

(35) Simonson, T. Gaussian fluctuations and linear response in an electron transfer protein. *Proc. Natl. Acad. Sci.* **2002**, *99*, 6544–6549.

(36) Reynolds, L.; Gardecki, J. A.; Frankland, S. J. V.; Maroncelli, M. Dipole solvation in nondipolar solvents: Experimental studies of reorganization energies and solvation dynamics. *J. Phys. Chem.* **1996**, *100*, 10337–10354.

(37) Terrettaz, S.; Cheng, J.; Miller, C. J. Kinetic parameters for cytochrome *c* via insulated electrode voltammetry. *J. Am. Chem. Soc.* **1996**, *118*, 7857–7858.

(38) Cheng, J.; Terrettaz, S.; Blankman, J. I.; Miller, C. J.; Dangi, B.; Guiles, R. D. Electrochemical comparison of heme proteins by insulated electrode voltammetry. *Israel J. Chem.* **1997**, *37*, 259–266.

(39) Wei, J. J.; Liu, H.; Niki, K.; Margoliash, E.; Waldeck, D. H. Probing electron tunneling pathways: Electrochemical study of rat heart cytochrome *c* and its mutant on pyridine-terminated SAMs. *J. Phy. Chem. B* **2004**, *108*, 16912–16917.

(40) Khodadadi, S.; Malkovskiy, A.; Kisliuk, A.; Sokolov, A. P. A broad glass transition in hydrated proteins. *Biochim. Biophys. Acta* **2010**, *1804*, 15–19.

(41) Ghorai, P. K.; Matyushov, D. V. Solvent reorganization entropy of electron transfer in polar solvents. *J. Phys. Chem. A* **2006**, *110*, 8857–8863.

(42) Dinpajooh, M.; Martin, D. R.; Matyushov, D. V. Polarizability of the active site of cytochrome *c* reduces the activation barrier for electron transfer. *Sci. Rep.* **2016**, *6*, 28152.

(43) Bortolotti, C. A.; Amadei, A.; Aschi, M.; Borsari, M.; Corni, S.; Sola, M.; Daidone, I. The reversible opening of water channels in cytochrome *c* modulates the heme iron reduction potential. *J. Am. Chem. Soc.* **2012**, *134*, 13670–13678.

(44) Martin, D. R.; Matyushov, D. V. Electron-transfer chain in respiratory complex I. *Sci. Rep.* **2017**, *7*, 5495.

(45) Mittal, J.; Hummer, G. Static and dynamic correlations in water at hydrophobic interfaces. *Proc. Natl. Acad. Sci. USA* **2008**, *105*, 20130–20135.

(46) Sarupria, S.; Garde, S. Quantifying water density fluctuations and compressibility of hydration shells of hydrophobic solutes and proteins. *Phys. Rev. Lett.* **2009**, *103*, 037803.

(47) Martin, D. R.; Matyushov, D. V. Dipolar nanodomains in protein hydration shells. *J. Phys. Chem. Lett.* **2015**, *6*, 407–412.

(48) Svergun, D. I.; Richard, S.; Koch, M. H. J.; Sayers, Z.; Kuprin, S.; Zaccai, G. Protein hydration in solution: Experimental observation by x-ray and neutron scattering. *Proc. Natl. Acad. Sci.* **1998**, *95*, 2267–2272.

(49) Lerbret, A.; Hédoux, A.; Annighöfer, B.; Bellissent-Funel, M.-C. Influence of pressure on the low-frequency vibrational modes of lysozyme and water: A complementary inelastic neutron scattering and molecular dynamics simulation study. *Proteins: Structure, Function, and Bioinformatics* **2012**, *81*, 326–340.

(50) Nibali, V. C.; D'Angelo, G.; Paciaroni, A.; Tobias, D. J.; Tarek, M. On the coupling between the collective dynamics of proteins and their hydration water. *J. Phys. Chem. Lett.* **2014**, *5*, 1181–1186.

(51) Böttcher, C. J. F. *Theory of Electric Polarization*; Elsevier: Amsterdam, 1973; Vol. 1.

(52) Matyushov, D. V.; Richert, R. Communication: Temperature derivative of the dielectric constant gives access to multipoint correlations in polar liquids. *J. Chem. Phys.* **2016**, *144*, 041102.

(53) Samara, G. A. The relaxational properties of compositionally disordered ABO_3 porovsketes. *J. Phys.: Condens. Matter* **2003**, *15*, R367–R411.

(54) Jung, Y.; Marcus, R. A. Protruding interfacial OH groups and 'on-water' heterogeneous catalysis. *J. Phys.: Condens. Matter* **2010**, *22*, 284117.

(55) Davis, J. G.; Rankin, B. M.; Gierszal, K. P.; Ben-Amotz, D. On the cooperative formation of non-hydrogen-bonded water at molecular hydrophobic interfaces. *Nat. Chem.* **2013**, *5*, 796–802.

(56) Matyushov, D. V. Electrophoretic mobility without charge driven by polarisation of the nanoparticle–water interface. *Mol. Phys.* **2014**, *112*, 2029–2039.

(57) Warshel, A.; Weiss, R. M. An empirical valence bond approach for comparing reactions in solutions and in enzymes. *J. Am. Chem. Soc.* **1980**, *102*, 6218–6226.

(58) Warshel, A. *Computer modeling of chemical reactions in enzymes and solutions.*; Wiley Interscience: New York, 1991.

(59) Landau, L. D.; Lifshits, E. M. *Statistical Physics*; Pergamon Press: New York, 1980.

(60) Schirò, G.; Cupane, A. Anharmonic activations in proteins and peptide model systems and their connection with supercooled water thermodynamics. *Il Nuovo Cimento* **2016**, *39 C*, 305.

(61) Zhang, C.; Galli, G. Dipolar correlations in liquid water. *J. Chem. Phys.* **2014**, *141*, 084504–6.

(62) Chau, P. L.; Hardwick, A. J. A new order parameter for tetrahedral configurations. *Mol. Phys.* **1998**, *93*, 511–518.

(63) Errington, J. R.; Debenedetti, P. G. Relationship between structural order and the anomalies of liquid water. *Nature* **2001**, *409*, 318–321.

(64) Nayar, D.; Agarwal, M.; Chakravarty, C. Comparison of tetrahedral order, liquid state anomalies, and hydration behavior of mTIP3P and TIP4P water models. *J. Chem. Theory Comput.* **2011**, *7*, 3354–3367.

(65) Biroli, G. A crash course on ageing. *J. Stat. Mech.* **2005**, P05014.

(66) Martin, D. R.; Matyushov, D. V. Communication: Microsecond dynamics of the protein and water affect electron transfer in a bacterial bc_1 complex. *J. Chem. Phys.* **2015**, *142*, 161101.

(67) Frauenfelder, H.; Chen, G.; Berendzen, J.; Fenimore, P. W.; Jansson, H.; McMahon, B. H.; Stroe, I. R.; Swenson, J.; Young, R. D. A unified model of protein dynamics. *Proc. Natl. Acad. Sci. USA* **2009**, *106*, 5129–5134.

(68) Seyedi, S.; Matyushov, D. V. Ergodicity breaking of iron displacement in heme proteins. *Soft Matter* **2017**, *13*, 8188–8201.

(69) Hales, B. J. Temperature dependency of the rate of electron transport as a monitor of protein motion. *Biophys. J.* **1976**, *16*, 471.

(70) Volk, M.; Aumeier, G.; Langenbacher, T.; Feick, R.; Ogrodnik, A.; Michel-Beyerle, M.-E. Energetics and mechanism of primary charge separation in bacterial photosynthesis. A comparative study on reaction centers of Rhodobacter sphaeroides and Chloroflexus aurantiacus. *J. Phys. Chem. B* **1998**, *102*, 735–751.

(71) Xu, Q.; Gunner, M. R. Temperature dependence of the free energy, enthalpy, and entropy of $P^+Q_A^-$ charge recombination in *Rhodobacter sphaeroides* R-26 reaction centers. *J. Phys. Chem. B* **2000**, *104*, 8035–8043.

(72) Jimenez, R.; Fleming, G. R.; Kumar, P. V.; Maroncelli, M. Femtosecond solvation dynamics of water. *Nature* **1994**, *369*, 471.